Applied Catalysis B: Environmental 195 (2016) 112–120

Contents lists available at ScienceDirect

Applied Catalysis B: Environmental

journal homepage: www.elsevier.com/locate/apcatb

Zirconium dioxide nanopowders with incorporated Si^{4+} ions as efficient photocatalyst for degradation of trichlorophenol using simulated solar light

M.V. Carević[a], N.D. Abazović[a], T.B. Novaković[b], V.B. Pavlović[c], M.I. Čomor[a,*]

[a] Vinča Institute of Nuclear Sciences, University of Belgrade, P.O. Box 522, 11001 Belgrade, Serbia
[b] IChTM- Department of Catalysis and Chemical Engineering, University of Belgrade, Njegoševa 12, 11000 Belgrade, Serbia
[c] Institute of Technical Sciences of Serbian Academy of Sciences and Arts, University of Belgrade, Knez Mihailova 35/IV, 11000 Belgrade, Serbia

ARTICLE INFO

Article history:
Received 2 March 2016
Received in revised form 1 May 2016
Accepted 3 May 2016
Available online 6 May 2016

Keywords:
Zirconia
Triclorophenol-TCP
Photocatalysis
Surface modification
Super oxide radicals

ABSTRACT

We present a hydrothermal method for synthesis of zirconia nanopowders: pure and with incorporated Si^{4+} ions. Zirconyl chloride and tetraethyl orthosilicate were used as precursors. As prepared powders were annealed at 600 °C and characterized using structural (XRD), morphological (SEM and TEM) and optical techniques (UV/vis DR, FTIR and photoluminescence spectroscopy). Their textural properties (BET method) and photocatalytic activity toward degradation of model compounds (tricholophenol and Rhodamine B) using simmulated solar light were obtained. We showed that by using hydrothermal synthesis method pure monoclinic ZrO_2 highly crystalline powder can be obtained. Incorporation of Si^{4+} ions induced stabilization of tetragonal crystalline phase at room temperature and decreasing of particle sizes. Incorporation of Si^{4+} ions in zirconia matrix also resulted in increase of specific area of nanopowders. FTIR measurements were used as proof for existence of Zr—O—Si bond. Effective band gap of zirconia powders was reduced from 5 (pure ZrO_2) to 3.8 eV for samples with Si^{4+} ions. All zirconia powders showed significant photocatalytic activity regarding degradation of triclorophenol and no activity regarding RB (Rhodamine B dye). Photocatalytic activity of zirconia was increased by incorporation of Si ions in the host matrix. The source of this observation is discussed correlating all obtained properties of pure and Si-incorporated nanopowders. Optimization of synthesis parameters and composition of zirconia samples obviously can lead to their photocatalytic activity comparable to Degussa TiO_2 powder, famous and commercial photocatalyst.

1. Introduction

The state of our planet is closely dependent on a development of new and renewable energy sources capable of overcoming the present strong dependence on fossil fuels, which are generating severe environmental damage [1]. A new ideal source should be inexpensive, abundant and clean. These criteria are met by sunlight since the Sun irradiates the Earth surface with a power of about 120,000 TW, much more (four orders of magnitude) than the current energy use on our planet [2]. It is not surprising therefore that a big effort has been done to orient the scientific research towards the exploitation of the solar light in various ways. This has occurred also within the catalytic community which is currently more and more oriented towards studies directed to exploit light in various kinds of applications [3]. Several practical applications of environmental photocatalysis are nowadays available (indoor air purification [4], water decontamination [5]), but the large scale commercial production of solar fuels is still a dream due to the difficulty in finding suitable artificial systems having high efficiency, long term stability and low cost. The basic component of a photocatalytic system is a semiconductor capable of generating a phenomenon of charge separation by absorbing light. The electron (excited in the conduction band) and the hole (consequently formed in the valence band) are potentially the agents of a reduction and of an oxidation reaction respectively [6]. Due to the intrinsic obstacles for appearance of these reactions, the whole system is in some cases integrated by a reduction and an oxidation co-catalyst. To achieve high performances of the whole photocatalytic system it is necessary to develop semiconductors having excellent electronic properties and, in parallel, co-catalysts

* Corresponding author.
E-mail address: mirjanac@vinca.rs (M.I. Čomor).

http://dx.doi.org/10.1016/j.apcatb.2016.05.005
0926-3373/

having high efficiency. Among the semiconductors employed in photocatalytic reactions, transition metal oxides play an important role due to their qualities in terms of stability in various media often accompanied by low or reasonable cost. The search for innovative materials in this field is oriented toward selection of systems having a suitable electronic structure capable of harvesting solar light at the earth surface (which means essentially visible light) and excellent potential to perform the desired redox process. This is practically hard to find in an unique system. Large band gap values correspond usually to good reductive and oxidative potentials, but these semiconductors also need high energy photons (UV light, scarcely present in solar light reaching the earth surface) to perform the charge separation. On the other hand, semiconductors with smaller band gap value, compatible with visible light absorption, cannot have satisfactory potentials for both reduction and oxidation of water or other useful reactions. To overcome this limitation, many approaches have been developed; for example coupling two different semiconductors in a so called Z-scheme, (each semiconductor deals with one of the two semi-reaction) a scheme directly inspired to natural photosynthesis [2]. An alternative possibility is to modify a semiconductor with relatively large band gap in order to make possible the absorption of visible light. This has been intensely studied in the case of titanium dioxide, the most used and investigated solid in the field of photocatalysis, following more than one approach (incorporation with transition metal ions [7], anchoring small metal particles exhibiting plasmonic effects [8], incorporation with non-metal atoms [9,10]) and with contradictory results.

Zirconia (ZrO_2) is one member of this group of wide band gap materials (besides TiO_2, ZnO for example). ZrO_2 is an important ceramic material widely used as a catalyst and catalyst support [11], sorbent [12], oxygen sensor [13] and solid oxide fuels [14]. Due to its nature as n-type semiconductor, it has been considered recently as a photocatalyst in photochemical heterogeneous reactions. The reported values of the bandgap energy (E_g) is in the range between 3.25 and 5.1 eV [15,16], depending on the used preparation technique and the presence of dopants and defects. From these, the most frequent and accepted value is 5.0 eV, with a conduction band potential of −1.0 V and the corresponding value of the valence band potential is +4.0 V vs. NHE at pH 0 [17]. The relatively wide E_g value and the high negative value of the conduction band potential allowed its use as a photocatalyst in the production of hydrogen through water decomposition [18]. Although pure ZrO_2 presents an absorption maximum around 250 nm, some samples show a non-negligible extrinsic absorption in the near UV and visible range due to the presence of so called color centers/defects in the zirconia matrix [19]. Recently, it was reported that zirconia nanostructures can be used for photocatalytic degradation of dyes [16,17,20], phenol [21] using light with energies larger than the intrinsic band gap energy of zirconia. It is proposed that different impurity bands and defect intraband states are responsible for its photoactivity [17,19,22].

The objective of this publication was to synthesize zirconia nanopowders with high specific surface without surfactants/additives, for photocatalytic application. We choose hydrothermal method for synthesis because it can be easily controlled and reproducible, it can be carried out at moderate temperatures and it already has been used to prepare nanosized powders [for example: 16, 20]. In order to gain as high specific surface as possible we introduced Si^{4+} ions in zirconia matrix during synthesis. Obtained materials were characterized and possibility of their photocatalytic application has been checked in the photodegradation processes of model compounds.

2. Experimental

The following commercial reagents were used: Zirconyl chloride octahydrate (reagent grade, SigmaAldrich, 98%), Tetraethyl orthosilicate (Aldrich, 98%), Rhodamine B (RB, Sigma, ≈95%), 2,4,6-Trichlorophenol (TCP, Alpha Aesar, 98%), Nitric acid (J.T. Baker, 65%) and Isopropanol (J.T. Baker, >99.8%), Sodium hydroxide (Aldrich, ≥97%), Methanol (Panreac, 99.9%), Titanium dioxide P25 (Degussa, >99.5%). All chemicals were used as received. In all experiments deionized water from Mili Q system was used.

2.1. Photocatalyst preparation

Pure and Si^{4+} incorporated zirconia nanopowders were synthesized by hydrothermal treatment. In a Teflon vessel (125 ml volume) 50 ml of 2 M NaOH, 2 g of zirconyl chloride powder for pure ZrO_2 (6.2 mM), and appropriate amount of TEOS for powders with Si^{4+} ions (0.5 ml–2.3 mM or 5 ml–23 mM, samples ZrO_2-1 and ZrO_2-2, respectively) were added. Dispersion was vigorously stirred for 1 h and then autoclaved for 24 h at 150 °C. The obtained powder was washed using water until the water reached pH = 7. Finally, the powder was separated from the washing solution by centrifugation. Synthesized powders were dried at 70 °C until attainment of constant weight. Finally, powders were calcined in an oven, at 600 °C for 3 h. Hydrothermal synthesis procedure was employed as a faster and more reproducible version of previously described procedures that involve reflux systems [23] for zirconia powders with high active surface.

2.2. Photocatalysts characterization

The XRD powder patterns were obtained by using a Philips PW 1050 powder diffractometer with Ni filtered Cu Kα radiation (λ = 1.5418 Å). The diffraction intensity was measured by the scanning technique (a step size of 0.05° and a counting time of 50 s per step). The average crystallite size (D in nm) was determined from XRD spectra according to the Debye-Scherrer Eq. (1):

$$D = \frac{k\lambda}{\beta \cos\theta} \quad (1)$$

where k is a constant equal to 0.89, λ is the X-ray wavelength equal to 0.15418 nm, β is the full width at half maximum intensity (FWHM) and θ is the diffraction angle (rad) of the most prominent peak for the obtained crystalline phase: (−111) at 2θ = 28.2° for monoclinic and (101) at 2θ = 30.2° for tetragonal crystalline phase.

UV/vis absorption and reflectance spectra of pure and Si-incorporated ZrO_2 powders were obtained using an Evolution 600 spectrophotometer (Thermo Scientific). Photoluminescence measurements were performed using PerkinElmer LS 45 fluorescence spectrometer.

Infrared spectra were taken using attenuated total reflection (ATR) mode of a Nicolet 380 FTIR spectrometer equipped with a Smart Orbit™ ATR attachment.

The morphology and sizes of photocatalysts were obtained using transmission electron microscopy, TEM, JEOL JEM 1400, accelerating voltage 120 kV.

The percent of incorporated Si^{4+} ions in ZrO_2 matrix was measured using scanning electron microscopy with energy dispersive X-ray spectroscopy, SEM/EDS, model: JEOL JSM-6610LV with EDS detector (model: X-Max Large Area Analytical Silicon Drift connected with INCA Energy 350 Microanalysis System).

Textural properties of our samples were determined using nitrogen adsorption/desorption parameters. The nitrogen adsorption was performed at −196 °C and relative pressure interval between 0.05 and 0.98 in automatic adsorption apparatus (Sorptomatic 1990 Thermo Finningen). Before each measurement, the sample was

degassed at 200 °C under vacuum for time enough (4 h < t < 10 h) to observe the absence of significant changes in vacuum stability. The adsorbed amount of nitrogen was measured by volume at standard temperature and pressure. The specific surface areas S_{BET} and C were calculated by the BET method [24–26] from nitrogen adsorption-desorption isotherms, using data up to $p/p_o = 0.3$, and the pore size distribution have been computed from desorption branch of the isotherms [26].

2.3. Photodegradation procedure

Photocatalytic degradation procedure was carried out as follows: at atmospheric pressure and room temperature 20 mg of synthesized photocatalyst, and Degussa for comparison, was added in 40 cm^3 of RB or TCP aqueous solution (concentrations: 5×10^{-5} and 5×10^{-4} mol/dm^3, respectively), at natural pH ~ 7. Before illumination, the mixture was stirred in the dark for one hour in order to achieve the adsorption-desorption equilibrium. Reaction suspension was constantly bubbled with O_2 and magnetically stirred during irradiation. Suspensions were placed into a vessel which was exposed to white light from an Osram Vitalux lamp (300 W, Sun light simulation, white light: UVB radiated power from 280 to 315 nm 3.0 W; UVA radiated power 315–400 nm 13.6 W; the rest is visible light and IR). Optical power was measured using R-752 Universal Radiometer read out with sensor model PH-30, DIGIRAD and it was ~ 30 $mWcm^{-2}$ at a distance of 30 cm from experimental solutions (used in this study) [27]. The aliquots (1 cm^3) were taken from the suspension and centrifuged.

2.4. Analytical procedure

For kinetic studies of RB and TCP photodegradation, using UV/vis spectroscopy and high performance liquid chromatography with diode array detection (HPLC), aliquots (1 cm^3) of the reaction mixture were taken at the beginning of the experiment and at regular time intervals. Each aliquot was than centrifuged. Supernatants were separated and UV/vis spectra were measured when degradation of RB was followed. RB has characteristic peak in UV/vis spectra with maximum at 550 nm. Aliquots extracted from TCP/catalyst suspensions were diluted with 1 ml of methanol and filtered through Agilent Technologies Econofilter 25/0.2 μm PTFE (syringe filter). The absence of the TCP adsorption on the filter was preliminarily checked.

After that, a 10 μl sample was injected and analyzed on an UltiMate 3000HPLC System, equipped with a UV–vis DAD set at characteristic wavelength of absorption maximum of TCP and at 292 nm and a Hypersil GOLD (250 mm × 4.6 mm i.d., particle size 5 μm, 21 °C) column. The mobile phase (flow rate 1 cm^3/min) was a mixture of methanol and water (7:3). In repeated runs, the results agreed within 5–10%.

3. Results and discussion

3.1. Structural, morphological and textural characterization of zirconia samples

Fig. 1 shows typical XRD patterns of pure ZrO_2 powder and ZrO_2 powders with incorporated Si ions. The pure ZrO_2 powder has peaks that can be indexed as monoclinic-ZrO_2 (Baddeleyite-JCPDS 65-1025) (Fig. 1(a)). Monoclinic ZrO_2 is the stable phase formed at temperatures less than 1170 °C in the absence of additives (where it transforms to tetragonal and then to cubic phase at temperatures above 2370 °C up to the melting point at 2680 °C) [28,29]. ZrO_2 nanopowders with incorporated Si ions are much less crystalline with broad peaks, Fig. 1(b), which can be assigned to

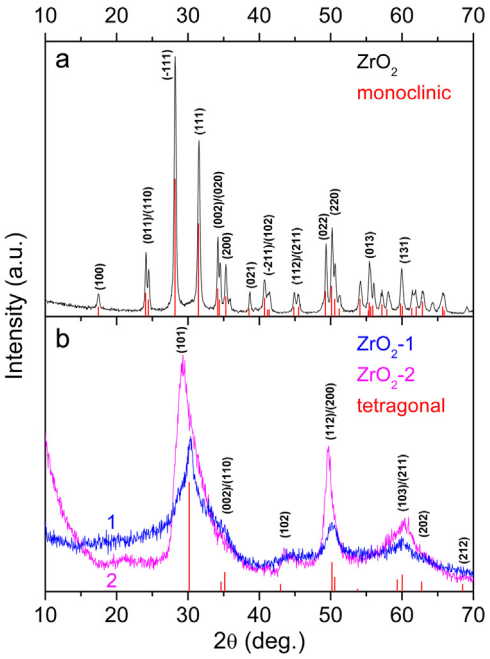

Fig. 1. XRD patterns of (a) pure ZrO_2 and (b) ZrO_2 with incorporated Si^{4+} ions.

tetragonal crystalline structure (JCPDS 81-1544). Cubic and tetragonal crystalline phase of ZrO_2 have very similar XRD pattern, the majority of peaks are at the same 2θ values while peaks at about 34°, 50°, 59° are doublet for tetragonal phase (JCPDS 81-1544 for tetragonal phase and JCPDS 89-9069 for cubic phase). XRD peak broadening is typical for crystal domains of few nanometers and consequently, it is hard to distinguish doublets from single peaks. However, according to literature data, incorporation of Si ions in zirconia lattice leads to stabilization of tetragonal crystal phase [29,30]. Additionally, at about 43° weak and broad peak, characteristic exclusively for tetragonal phase is present, and is considered as proof of tetragonal phase stabilisation. ZrO_2-1 had still, to some extent, monoclinic phase which moved the most intensive peak to lower 2θ values. Powder with higher concentration of Si ions even showed a mixture of t-ZrO_2 and amorphous SiO_2; the halo at approximately 2θ = 22° corresponds to amorphous SiO_2. Particle sizes were calculated using Debye-Scherrer equation as stated in Section 2. Pure ZrO_2 had diameters of about 25 nm and both samples with incorporated Si ions had diameters of about 3 nm.

As reported previously, the monoclinic phase is the stable phase at low temperatures, but the tetragonal phase is the first formed in nucleation process and heat treatment [30]. The presence of the metastable tetragonal phase at low temperatures can be attributed to several factors such as chemical effects (the presence of anionic impurities), structural similarities between the tetragonal phase and the amorphous zirconia phase that is precursor of crystallization, as well as particle size effects (based on the lower surface energy in the tetragonal phase compared to the monoclinic phase). This last argument is based on Ostwald's rule, which states that when a substance can exist in more than one form, the least stable state occurs first [30]. The presence of lattice strains and defect centres in the crystalline structure do not allow the t → m transformation to occur below a fixed critical particle size, about 30 nm for pure ZrO_2. Our pure ZrO_2 powder sample obviously, had crystallites of appropriate sizes (~25 nm) but samples with incorporated Si ions had much smaller particles, almost 10 times smaller than critical value. These lattice strains and defect centres can be a consequence of the crystallization of the tetragonal phase from amorphous zirconia as well as by the presence of chemical impurities. So, the

Table 1
Textural properties, calculated band gaps from Tauc's plots and composition of sinthesized zirconia samples (determined using SEM/EDX).

Sample, E_{bg} [eV]	S_{BET}, [$m^2\ g^{-1}$]	D_{max1}, [nm]	D_{max2}, [nm]	$V_{p\ 0.98}$, [$cm^3\ g^{-1}$]	$V_{p\ micro}$, [$cm^3\ g^{-1}$]	Zr, [mol%]	Si, [mol%]
ZrO_2 ~5	23	50	/	0.189	/	/	/
ZrO_2-1 ~4.7	160	3.8	0.9	0.473	0.080	85	15
ZrO_2-2 ~3.8	138	7	0.6	0.438	0.050	60	40

presence of Si ions in samples 1 and 2, led to formation of Zr—O—Si bonds and/or the formation of a thin silica layer surrounding the zirconia particles (sample ZrO_2-2) which is enough to preserve the particle growth. The occurrence of such an effective constrained effect for just a thin silica layer surrounding the zirconia particles must be due to the amorphous character of the silica, allowing a large contact surface between the zirconia particles and the surrounding silica.

On heating, zirconia has to diffuse through the thin layer of silica to nucleate in order to form crystalline particles. Thus, first appearance of Si incorporated in crystalline particles as well as growth to their critical particle size needs temperatures higher that 600 °C that we used for annealing of our samples. Similar observations have been published by del Monte et al. [30]. They studied a several ZrO_2–SiO_2 composites and stated that even 2 mol% of Si ions in ZrO_2 matrix can suppress crystallization process (from 450 °C for pure ZrO_2 to more than 500 °C for composite) as well as phase transformation (from 550 °C to about 1000 °C). Also the critical size for t → m transformation was increased from 26.5 nm for pure ZrO_2 to 39 nm for composite with 2 mol% of Si. Vasanthavel et al. [29] studied influence of SiO_2 content on the crystalline phase content of ZrO_2 matrix. They found that silica can have important role in stabilization of low temperature tetragonal phase, especially when silica is present in the majority; when zirconia is spread in amorphous silica matrix. Our samples had higher content of Si ions in zirconia matrix (ZrO_2-1 ~15 mol% and ZrO_2-2 ~40 mol%, Table 1) compared to results presented by Vasanthavel et al. [29], and these effects were even more pronounced, especially in the case of ZrO_2-2 for which amorphous silica was detected in the XRD (Fig. 1).

In Fig. 2 a typical TEM images of pure zirconia (a) and zirconia powders with incorporated Si ions (b and c) are presented. Pure ZrO_2 is constituted of large particles, $D \geq 20$ nm and even larger agglomerates of about 100 nm, although this size should be taken cautiously as it was difficult to distinguish boundaries between entities. These findings are in agreement with diameter/sizes of crystallites calculated from XRD. Crystalline domains gained using Debye-Scherrer equation can be smaller than real sizes of the particles due to presence of amorphous phase present as well. In addition to well defined crystal nanoparticles, with visible crystal planes, some defects can also be observed like pits with diameters of 5–10 nm. These pits are small amorphous zones embedded in the crystalline zirconia matrix [31].

In Fig. 2b and c small particles of 3–6 nm can be seen in both samples with Si ions, ZrO_2-1 and ZrO_2-2, with sizes in agreement to those calculated using Debye-Scherrer equation. Also some larger elongated particles/agglomerates ($D \sim 20$ nm) with defect/twinned structure can be observed. In these larger particles with twinned domains, most probably started the t → m transformation [32], but the volume fraction of monoclinic crystalline phase still being too low in order to be registered by XRD. It can be seen that Si incorporation process suppress effectively the growth of nanoparticles trough hydrothermal synthesis process and subsequent annealing as was proposed by Monte et al. [30] in the case of ZrO_2–SiO_2 binary oxides prepared using sol-gel route, without hydrothermal synthesis step.

In addition to XRD and TEM measurements particle sizes are calculated from textural properties of the samples. Results are listed in Table 1, together with their chemical composition measured using

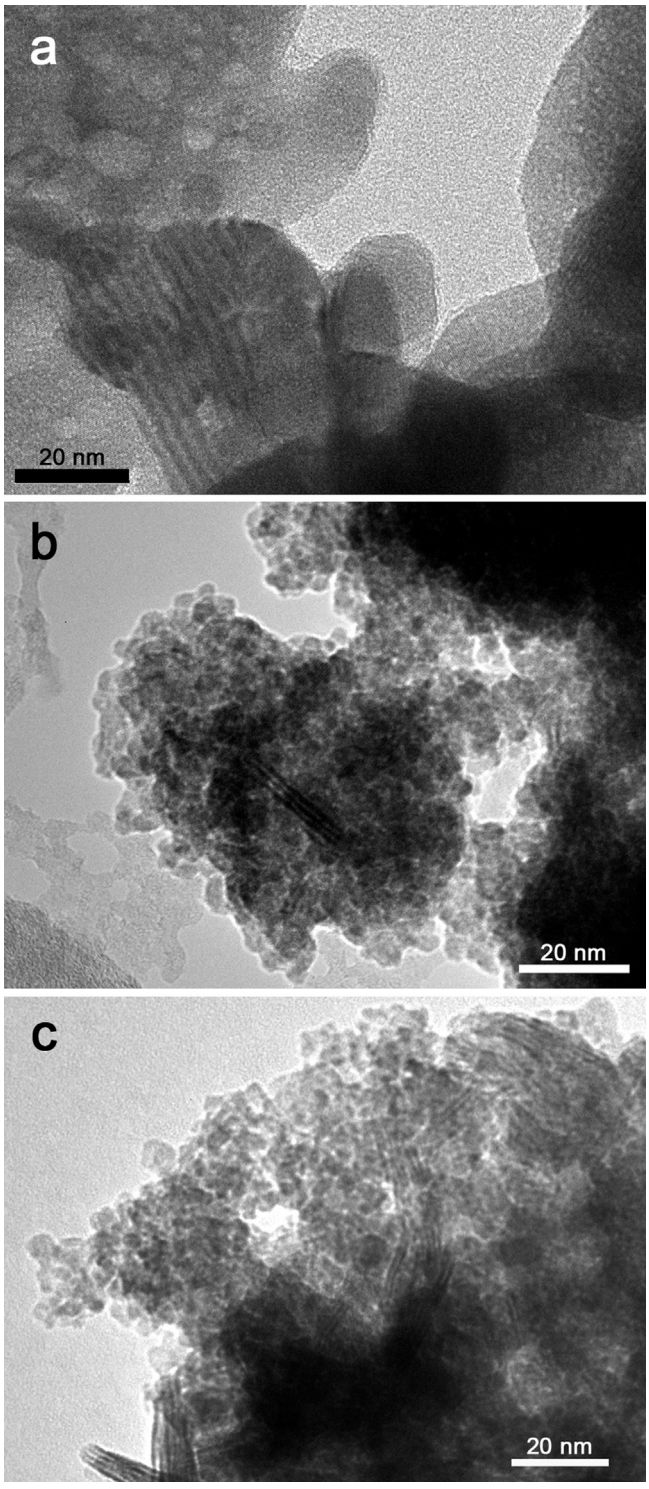

Fig. 2. Typical TEM images of ZrO_2 based photocatalysts: (a) pure and (b, c) with incorporated Si^{4+} ions.

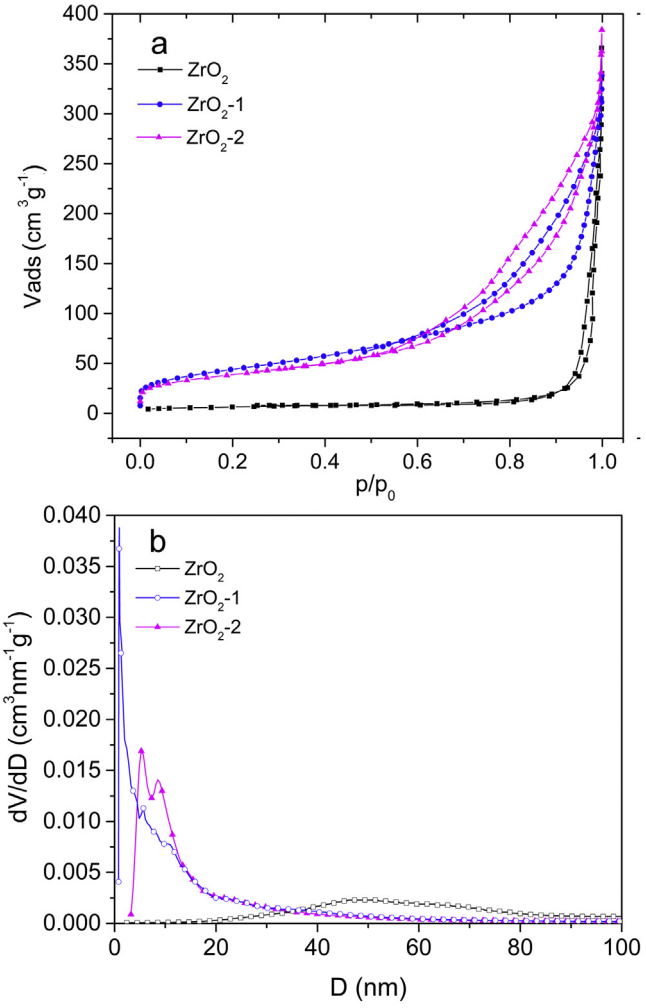

Fig. 3. (a) N_2 adsorption/desorption isotherms and (b) pore size distributions patterns of ZrO_2 samples.

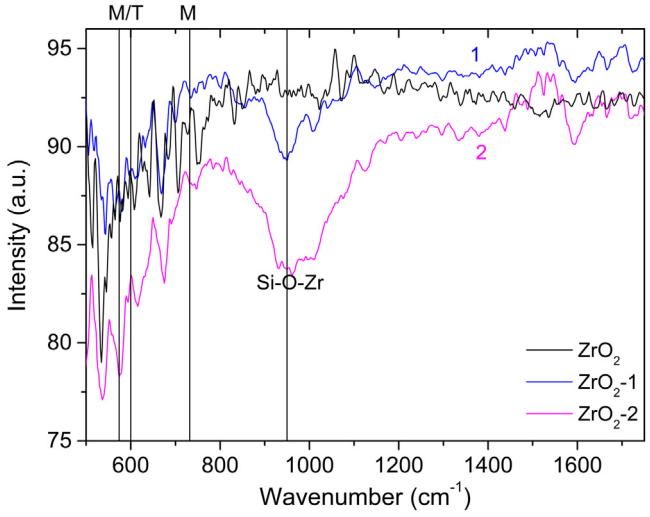

Fig. 4. FTIR spectra of pure and zirconia powders with incorporated Si^{4+} ions.

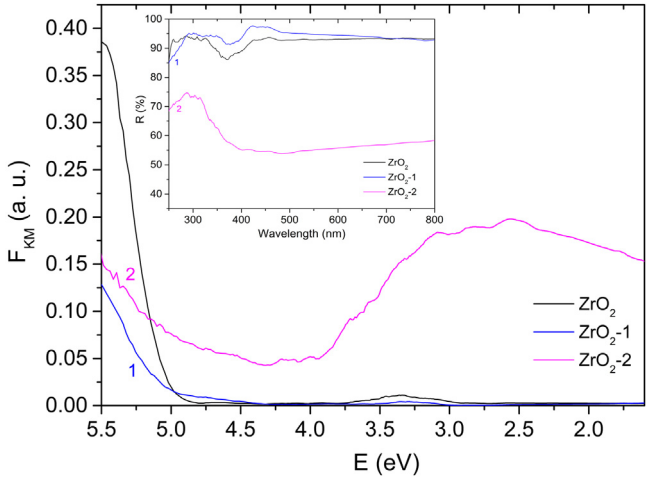

Fig. 5. UV/vis absorption and DRS (inset) spectra of pure zirconia and zirconia nanopowders with incorporated Si^{4+} ions.

SEM/EDX technique. All results are in fair agreement with each other.

Samples ZrO_2, ZrO_2-1 and ZrO_2-2 as a number of powders or aggregates, have isotherms shape type II, which exhibit type H3 hysteresis loop as can be seen in Fig. 3(a). The narrow hysteresis loop is the result of inter-particle capillary condensation (usually within a nonrigid aggregate). Type H3 loops are often given by the aggregates of platy particles [24]. ZrO_2 has a small specific surface area and large mean pore diameter, almost macroporous. ZrO_2-1 and ZrO_2-2 have very similar isotherms, i.e., the same shape of the pores, but different pore size distribution (different mean pore diameter, Fig. 3(b)) and the number of pores with same mean pore diameter (Table 1), causing the difference in the pore volume. Also, the specific surface areas of these samples are larger compared to specific surface area of the pure ZrO_2 sample. It can be concluded that incorporation of Si-ions in zirconia induced reduction of particle and pore sizes and increased the specific surface area, Fig. 3. That was one of the main goals that we wanted to achieve with this study. The specific surface area is slightly larger when smaller concentration of Si ions (15 mol%) was incorporated in zirconia matrix, as a consequence of saturation of particle surface with Si ions or presence of amorphous silica layer on the surface of the particles for sample ZrO_2-2. We would like to stress that comparing theoretical and actual mol% of Si ions can be seen that only small part of added Si ions can be incorporated in zirconia matrix. Even for initial reaction conditions with 4 times higher molar concentration of Si precursor compared to Zr precursor, only 40 mol% of Si ions was incorporated in ZrO_2 matrix.

3.2. Optical characterization of the zirconia samples

In order to prove formation of Zr—O—Si we measured FTIR of our samples. In Fig. 4 FTIR spectra of zirconia samples are presented in the wavenumber range where peaks typical for ZrO_2 and SiO_2 can be expected, from 500 to 1700 cm^{-1} [30]. Unfortunately, due to instrumental limitations, it was not possible to measure spectra below 500 cm^{-1}, where the most important peaks of tetragonal and monoclinic ZrO_2 crystal phase are; for t-ZrO_2:480 cm^{-1} which can be moved to 570–600 cm^{-1}; and for m-ZrO_2:354, 416, 498, 574 and 732 cm^{-1}. The most prominent peak for Si incorporated samples is at about 950 cm^{-1} and can be assigned to Zr—O—Si [33]. This finding can be used as a proof of the presence of Si^{4+} ions in the ZrO_2 matrix. In sample ZrO_2-2 a broadening of the peak at 950 cm^{-1} toward 1060 cm^{-1} can be observed due to possible formation of SiO_2. Broad band at 1060 cm^{-1} is characteristic of SiO_2 [30].

In Fig. 5. UV/vis absorption/reflection spectra of ZrO_2 powders are presented. The band gap energies calculated from Tauc's plots are given in Table 1. ZrO_2 is an active and typical photon absorber and photocatalyst among wide band gap metal oxides although

band gap excitation is in the UVC part of the spectra. It is a direct band gap material with two direct band to band transitions at 5.2 and 5.79 eV regarding to Kumar et al. [17], but the wide variety of data for band gap energies can also be found in literature from 5.1 to 3.25 eV [15,16,34–37]. The valence band of ZrO_2 is mainly composed of occupied 2p energy state of O atom and the conduction band is constituted by unoccupied 4d energy states of Zr atom [17]. The UV/vis spectrum of pure ZrO_2 sample (Fig. 5) shows an absorption raise toward wavelengths shorter than 250 nm, calculated value of band gap energy is 5 eV. That absorption band corresponds to valence band to conduction band (VB → CB) transition. The broad absorption (Fig. 5.) that can be observed for zirconia with Si ions, at the photon energies smaller than band gap of zirconia, can originate from the defect color centres from an overlap of several single absorption bands belonging to the electron color centres of the F, F^+, (oxygen vacancies with 2 or 1 electron), and Zr^{3+}-type displaying maxima at about 2.0 eV (620 nm), 3.0 eV (410 nm), and 4.5 eV (275 nm), respectively, and hole colour centers of the V-type with a maximum at 3.25 eV (380 nm) [19] which can also be assigned to newly formed states after incorporation of Si ions in the zirconia matrix. Mixtures of metal oxides optically inert in the visible part of the spectra can have new absorption threshold moved to much smaller energies compared to pure oxides [35]. As can be seen in Fig. 5 and Table 1, zirconia powders with Si ions have band gap energies of 4.7 eV (ZrO_2-1) and 3.8 eV (ZrO_2-2).

However, Navio et al. [36,37] reported an energy band gap of 3.7 eV for monoclinic ZrO_2 powders prepared by sol-gel method. These authors claim that the decrease in the band gap energy could be attributed to a highly disordered structure, as a result of the conditions used in the preparation technique. We suppose that is also an explanation for our findings, since hydrothermal method together with incorporation of Si^{4+} ions can provide favorable environment for production of highly defective materials. As a consequence of the presence of structural defects, some energy levels are introduced into the semiconductor band gap that allow transitions of lower energy and therefore lead to a decrease of the band gap energy. Similar observations were published by Gionco et al. [22] when ZrO_2 has been doped with Ce ions. All doped samples showed transitions with pronounced red shift of absorption, compared to bare zirconia, with significant tailing. So they concluded that Ce ions induced intra-band states (states based on Ce ions and oxygen vacancies) which contributed to zirconia visible light absorption [22].

PL spectroscopy is an extremely useful tool for obtaining the information about the electronic, optical and photoelectric properties of the materials. PL spectra depend strongly on the particle size, defects and impurities present in the materials. The PL spectra of pure ZrO_2 and ZrO_2 with incorporated Si^{4+} ions, are shown in Fig. 6.

The excitation wavelengths are chosen to be 240 nm/5.1 eV (Fig. 6a) and 350 nm/3.54 eV (Fig. 6b). It can be seen that both excitations give arise of broad emission bands. This indicates that the fluorescence involves the same initial and final states, even as the excitation wavelengths were varied, suggesting fast relaxation from the final state that is reached after photoexcitation to the states where fluorescence originates. The broad nature of spectral features strongly indicated that fluorescence involves defect/intraband/extrinsic states. When excitation energy exceeds the band gap of ZrO_2 nanoparticles (Fig. 6a), electron-hole pairs are produced. The electron can be trapped by the oxygen vacancies (V_O) and create F and F^+ centres. The Zr^{4+} ions adjacent to the bulk V_O could capture electrons forming Zr^{3+} ions [17]. Recombination of the holes with F centres creates the excited states of the emitter which than undergo radiative transitions to the ground state. If the main source of the defect centres in ZrO_2 are oxygen vacancies and Zr^{3+} interstitials we can expect emission bands with

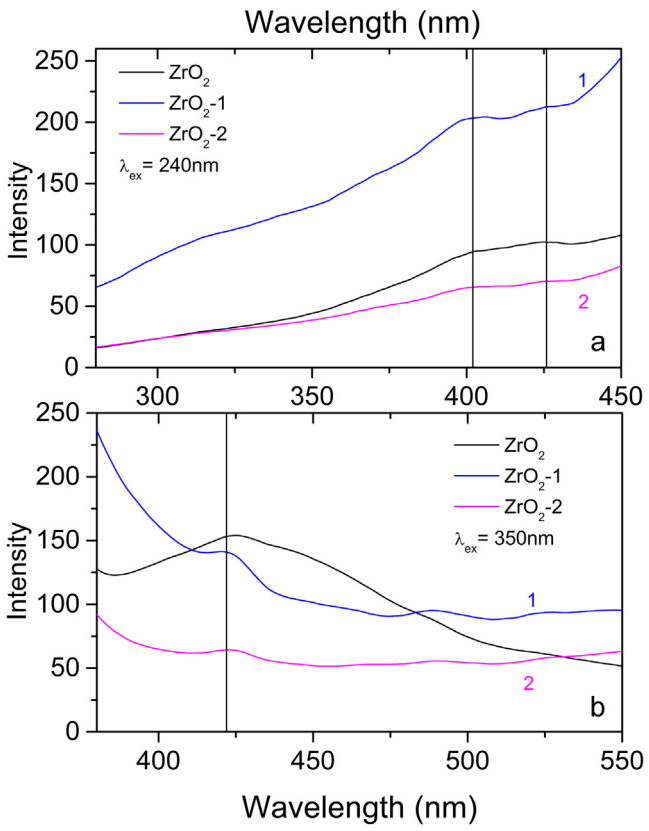

Fig. 6. PL spectra of ZrO_2 nanoparticles, using excitation wavelengths of 240 (a) and 350 nm (b).

peak/shoulders at about 380–400 nm [17]. Our results are similar, when we used higher energy photons for excitation of all zirconia samples (Fig. 6a) with addition of shoulder at about 425 nm. When we used 350 nm for excitation, photon energy lower than band gap of zirconia, only peak/shoulder at about 425 nm could be observed. That PL feature can be attributed to singly ionized oxygen vacancies in ZrO_2 nanoparticles, resulting emission band originates from radiative recombination of photogenerated hole and electron occupying V_O [17] and other defect and impurity states formed in zirconia during synthesis and incorporation of Si^{4+} ions.

3.3. Photocatalytic activity of zirconia based nanoparticles

In Fig. 7a kinetic curves of the photocatalytic degradation of TCP using pure ZrO_2 and ZrO_2 with incorporated Si^{4+}ions are presented. As can be seen all prepared photocatalysts can degrade TCP in given experimental conditions, with efficacies comparable to the most famous commercial Degussa TiO_2 photocatalyst. Degradation of 50% of TCP was achieved after about 2 h using pure ZrO_2 and after about 75 min when Si^{4+} incorporated ZrO_2 photocatalysts were used. Results obtained for ZrO_2-1 and ZrO_2-2 photocatalysts are similar: after 4 h of irradiation only less than 10% of initial concentration of TCP was present. The pure zirconia degraded about 75% of TCP after 4 h of irradiation.

Bearing in mind results already presented in this section, especially UV/vis spectra (Fig. 5), these findings are puzzling, the most of all for pure ZrO_2. In order to rule out the effect of adsorption we checked adsorption in the dark in the same time frame as photocatalysis, for all samples. Results obtained for 2 h of adsorption or irradiation are presented in Table 2. The differences between adsorption and photocatalysis are conclusive regarding of the process involved in the disappearance of TCP. In Table 2 rates of TCP

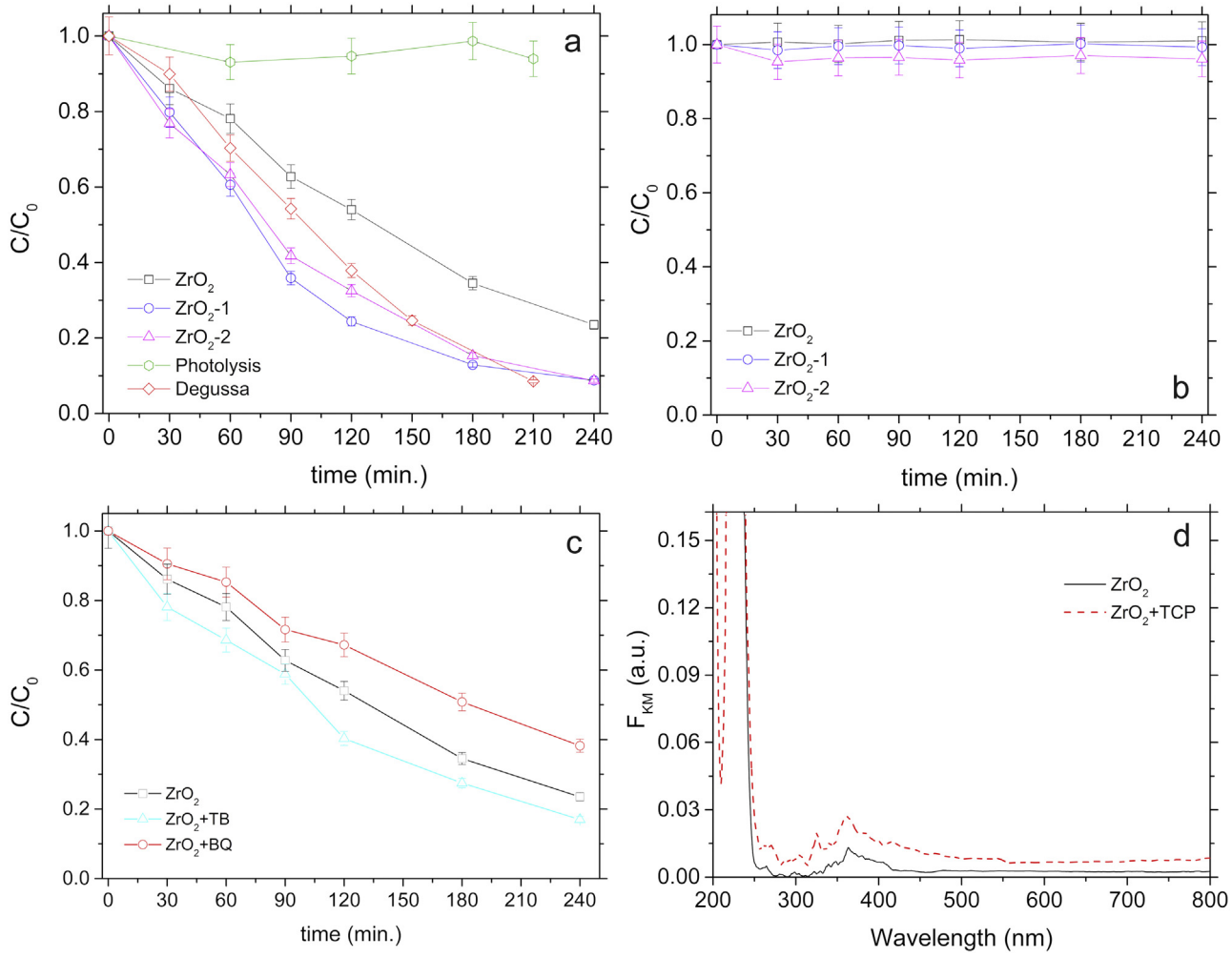

Fig. 7. Kinetic curves of (a) photolysis of TCP and photocatalytic degradation of TCP and (b) photolysis of RhB and photocatalytic degradation of RhB, using zirconia photocatalysts and Degussa for comparison; (c) Kinetic curves of photocatalytic degradation of TCP using pure ZrO_2 with and without radical scavengers: BQ and TB; (d) UV/vis absorption spectra of bare pure ZrO_2 and after adsorption of TCP on the surface of ZrO_2.

Table 2
The percent of adsorbed and photodegraded TCP when using pure and Si^{4+} incorporated ZrO_2 samples, after 2 h of adsorption in the dark or 2 h of irradiation with simulated solar light, respectively. The degradation rates (R) of TCP, determined at 2 h of irradiation in the presence of Degussa and studied zirconia photocatalysts are also presented.

	Adsorption (%)	Photocatalysis (%)	R (μmol/(dm^3 min))
ZrO_2-0	3	46	1.9
ZrO_2-1	10	75	3.1
ZrO_2-2	12	68	2.8
Degussa	/	63	2.6

degradation are also presented and one can see that all prepared catalysts can be used for efficient TCP photodegradation, although the best is ZrO_2-1 even when compared to Degussa, the most efficient commercial titania photocatalyst.

We also tested zirconia based photocatalysts for degradation of RB (Rhodamine B), results are presented in Fig. 7b. As can be seen, none of the applied photocatalysts showed any activity. The photodegradation procedure was conducting at natural pH (~7) at which ZrO_2 surface is partially negatively charged ($pH_{IEP} \sim 6$, [36]) same as RB which is in ionized form ($pK_a = 3$, [38]) and adsorption is, most probably, supressed. TCP has $pK_a = 5.99$ [39], better suited for adsorption and photocatalytic degradation on zirconia surface.

The applications of zirconium dioxide in photocatalysis are very few if compared to the commonly employed photocatalysts, like titanium dioxide. However some reports are available concerning both photocatalytic oxidations of chemicals [16,17,20,37], water photosplitting and carbon dioxide photoreduction [18,40].The band energy levels of ZrO_2 are in principle very suitable for photocatalytic applications. In particular the lowest potential of the conduction band is at about −1.0 V (vs. NHE, pH 0), i.e. much more negative than that of TiO_2 which is close to zero, and the highest potential in the valence band of ZrO_2 is around +4.0 V, i.e. quite more positive than that of TiO_2 (+2.95 V) [22]. The major drawback limiting the photocatalytic applications of ZrO_2 is its band gap value which is particularly high (5.0 eV). This value corresponds to UVC frequencies, necessary to perform charge separation, practically absent in the Solar radiation reaching the earth surface, thus dissuading from the search of practical applications of bare ZrO_2 using Sun light.

In order to explain obtained results we will present two major ways of photoactivation reactions over spectral ranges: intrinsic ($h\nu \geq E_{bg}$) and extrinsic absorption ($h\nu \leq E_{bg}$) [41]. The extrinsic absorption of light and formation of electron–hole pairs strongly depend on the optical properties of the defects and on the position of the ground (and excited) defect states in the band gap; there is no simple correlation between the optical properties of the dominating type of point defects and the electronic properties of

metal oxides. Second, under persistent light irradiation, each successive absorption event for a light quantum with $h\nu \geq Eg$ occurs in some arbitrary site of the particles, whereas each successive light absorption by the defects ($h\nu \leq E_{bg}$) occurs in a permanent albeit limited number of sites. As a result, the efficiency of the photoprocesses following photoexcitation of the solid, such as trapping and detrapping of charge carriers, diffusion to the surface and in the bulk, and surface/bulk electron–hole pair recombination, may differ significantly for processes following the intrinsic and extrinsic light absorption. Consequently, these differences may be reflected in the observed differences in the spectral dependencies of photocatalyst efficacy. In other words, active centres formed during photoexcitation in the extrinsic absorption spectral region are different from those formed from the intrinsic absorption of light and possess less oxidative power, which leads to changes in the reaction pathway. In some cases, the lesser power of such active centres may be insufficient to initiate the course of the reaction [41]. This can explain absorption of photons of lesser energy than the band gap of ZrO_2 obtained in our study and observed photocatalytic activity. Also we should consider possibility of surface modification of zirconia photocatalysts by TCP. As can be found in literature there are many similarities between titania and zirconia surfaces when we consider nanoparticles ($D \leq 5$ nm) [42]. Both surfaces can be modified using different organic molecules which have OH groups in their structure. Surface modification can lead to formation of charge transfer complexes which can induce significant improvement of extrinsic light absorption ($h\nu \leq E_g$). Hurum et al. [43] studied the reaction mechanism of TCP degradation using TiO_2 nanoparticles, by intrinsic and extrinsic light absorption. They found that no charge separation in the TiO_2 slurry can be observed at sub-bandgap energies and degradation of TCP in these experiments is not due to bandgap excitation of the catalyst. Instead, they suggest that a previously observed charge transfer complex between the catalyst and the TCP leads to the production of the phenoxy radical. In this case, an electron is donated from TCP to the catalyst, leaving the phenoxy radical of TCP on the surface as the first step in its degradation [43]. The extracted electron can than make a super oxide radical ($O_2^{\bullet -}$) which through series of reactions end up forming OH radicals which degrade TCP and phenoxy radicals as well. If we assume the similarities between TiO_2 and ZrO_2 [42] we can expect the same process at the surface of ZrO_2 and when extrinsic absorption occurs super oxide radicals are important in photocatalytic process we are studying. In order to gain some insight does our photocatalysts react in the same way we probed pure ZrO_2 photocatalytic degradation of TCP with radical scavengers: benzoquinone (BQ) as a scavenger for super oxide radicals and *tert*-butyl alcohol as a scavenger for hydroxyl radicals [44]. Our results are presented in Fig. 7c. Results suggest that when super oxide radicals are removed from the reaction, photodegradation rate of reaction slows down, and when the hydroxyl radicals are removed reaction speeds up. Removing of hydroxide radicals most probably block recombination process of photogenerated charge carriers, and improve transfer of electrons to adsorbed O_2.

In the study published by Karunakaran et al. [21], similar mechanism was proposed for photodegradation of phenol using ZrO_2 as a photocatalyst. They claimed that phenol and surface Zr sites can form charge-transfer complex which move apparent absorption threshold to lower energies compared to bare ZrO_2 nanoparticles. Recently, Bedilo et al. [45] studied formation of super oxide radicals on the surface of zirconia nanoparticles when hydrocarbons and molecular oxygen are coadsorbed. They claim that super oxide radical can be formed using visible light due to complex formation between Zr^{4+}/Zr^{3+} ions on the zirconia surface and hydrocarbon molecule, and subsequent electron transfer to adsorbed molecular oxygen. The most probable mechanism seems to be SIET- surface intermolecular electron transfer [45]. We obtained DRS spectrum of possible CT complex formed on the surface of the pure ZrO_2. Corresponding absorption spectrum, after Kubelka-Munk transformation, is presented in Fig. 7d. Slight improvement of absorption intensity towards longer wavelengths can be seen compared to bare ZrO_2. So, process of surface modification, together with presence of defect states in the band gap of ZrO_2 can be considered as a potential explanation for obtained photocatalytic activity, both reasons are possible in the case of pure ZrO_2 and later far more important in the case of samples with Si^{4+} ions.

All zirconia photocatalysts, with and without Si ions, have high photocatalytic activity regarding TCP degradation, although sample ZrO_2-1 is slightly better until the 3 h of irradiation. Samples with Si^{4+} ions reach the same value of the degradation (under 10% of the initial concentration of TCP was left) after 4 h of irradiation. Similar differences are obtained when S_{BET} results are compared. Pure ZrO_2 has the smallest S_{BET} (7–8 times smaller than Si incorporated samples), and its photocatalytic activity is lower compared to samples with Si ions. Obviously, for photocatalytic material the proper correlation of all parameters (crystalline phase, S_{BET}, the surface composition, defect and impurity states) is necessary. Hydrothermal method that we used for synthesis of zirconia based photocatalysts is obviously excellent for proper balance of defect/intraband states that are optically active even in the visible part of the spectra, which can be used in processes of photocatalytic degradation of pollutants.

4. Conclusions

The hydrothermal method was successfully used for synthesis of pure zirconia and zirconia with incorporated Si ions. Pure ZrO_2 had monoclinic crystalline phase and particles of about 20 nm, powders with incorporated Si ions remained in metastable tetragonal crystalline phase with diameters of about 3–6 nm. Significant increase of specific surface area was achieved by incorporation of Si ions in zirconia matrix- S_{BET} of powders with Si ions was 7 times larger than pure zirconia. FTIR measurements showed that incorporation of Si ions was achieved mostly through formation of Zr—O—Si bonds. Both, the hydrothermal method of synthesis and Si ions induced formation of different intraband states, for example oxygen vacancies, which moved absorption threshold of samples to lower energies: from 5 eV for pure zirconia to 4.7 and 3.8 eV for ZrO_2-1 and ZrO_2-2, respectively. The presence of intraband states was also proved using PL technique. This fact enabled more efficient usage of solar light for photocatalytic degradation of TCP. All synthesized powders can be used for photocatalytic degradation of TCP, the zirconia samples with incorporated Si ions were more efficient than Degussa commercial TiO_2 powder. Neither photocatalyst showed any activity toward degradation of RB. The main source of photocatalytic activity of obtained powders are most probably super oxide radicals ($O_2^{\bullet -}$) which than through several reactions resulted in degradation of TCP. These results are encouraging for future studies of zirconia based photocatalysts.

Acknowledgements

The authors are grateful to Dr Miodrag Mitrić for XRD measurements. Financial support for this study was granted by the Ministry of Education, Science and Technological Development of the Republic of Serbia (Project OI172056).

References

[1] G.A. Olah, G.K.S. Prakash, A. Goeppert, J. Am. Chem. Soc. 133 (2011) 12881–12898.
[2] J. Barber, Chem. Soc. Rev. 38 (2009) 185–196.
[3] K. Maeda, K. Domen, J. Phys. Chem. Lett. 1 (2010) 2655–2661.

[4] J. Lyu, L. Zhu, C. Burda, Catal. Today 225 (2014) 24–33.
[5] G.P. Anipsitakis, D.D. Dionysiou, Appl. Catal. B: Environ. 54 (2004) 155–163.
[6] A. Fujishima, X. Zhang, D.A. Tryk, Surf. Sci. Rep. 63 (2008) 515–582.
[7] M.I. Čomor, N.D. Abazović, I.A. Janković, D.J. Jovanović, M. Stoiljković, D.V. Šojić, B.F. Abramović, Rutile: Properties, Synthesis and Application, in: J. Low (Ed.), Nova Publishers, Inc., New York, 2012, pp. 29–51.
[8] S.C. Warren, E. Thimsen, Energy Environ. Sci. 5 (2012) 5133–5146.
[9] R. Asahi, T. Morikawa, T. Ohwaki, K. Aoki, Y. Taga, Science 293 (2001) 269–271.
[10] A.V. Emeline, V.N. Kuznetsov, V.K. Rybchuk, N. Serpone, Int. J. Photoenergy 2008 (2008) 19 (Article ID 258394).
[11] T. Yamaguchi, Catal. Today 20 (1994) 199–218.
[12] P.A. Deshpande, S. Polisetti, G. Madras, Langmuir 28 (2011) 3578–3587.
[13] T. Liu, X. Zhang, L. Yuan, J. Yu, Solid State Ion. 283 (2015) 91–102.
[14] J.H. Shim, C.C. Chao, H. Huang, F.B. Prinz, Chem. Mater. 19 (2007) 3850–3854.
[15] S. Chang, R. Doong, J. Phys. Chem. B 108 (2004) 18098–18103.
[16] S.N. Basahel, T.T. Ali, M. Mokhtar, K. Narasimharao, Nanoscale Res. Lett. 10 (2015) 73.
[17] S. Kumar, A.K. Ojha, J. Alloy Compd. 644 (2015) 654–662.
[18] K. Sayama, H. Arakawa, J. Phys. Chem. 97 (1993) 531–533.
[19] A.V. Emeline, G.N. Kuzmin, D. Purevdorj, V.K. Ryabchuk, N. Serpone, J. Phys. Chem. B 104 (2000) 2989–2999.
[20] Z. Shu, X. Jiao, D. Chen, CrystEngComm 14 (2012) 1122–1127.
[21] C. Karunakaran, R. Dhanalakshmi, P. Gomathisankar, Spectrochim. Acta A 92 (2012) 201–206.
[22] C. Gionco, M.C. Paganini, M. Chiesa, S. Maurelli, S. Livraghi, E. Giamello, Appl. Catal. A-Gen. 504 (2015) 338–343.
[23] S.F. Yin, B.Q. Xu, ChemPhysChem (2003) 277–281.
[24] F. Rouquerol, J. Rouquerol, K.S.W. Sing, P. Llewellyn, G. Maurin, Adsorption By Powders and Porous Solids, Principles Methodology and Applications, Academic Press, New York, 2012.
[25] B.C. Lippens, B.G. Linsen, J.H. de Boer, J. Catal. 3 (1964) 32–37.
[26] K. Sing, D. Everet, R. Haul, L. Moscou, R. Pierotti, J. Rouquerol, T. Siemieniewska, Pure Appl. Chem. 57 (1985) 603–619.
[27] M. Radoičić, Z. Šaponjić, I.A. Janković, G. Ćirić-Marjanović, S.P. Ahrenkiel, M.I. Čomor, Appl. Catal. B: Environ. 136–137 (2013) 133–139.
[28] J. Chevalier, L. Gremillard, A.V. Virkar, D.R. Clarke, J. Am. Ceram. Soc. 92 (2009) 1901–1920.
[29] S. Vasanthavel, P.N. Kumar, S. Kannan, J. Am. Ceram. Soc. 97 (2014) 635–642.
[30] F. Monte, W. Larsen, J.D. Mackenzie, J. Am. Ceram. Soc. 83 (2000) 628–634.
[31] C. Tiseanu, B. Cojocaru, V.I. Paravulescu, M. Sanchez-Dominguez, P.A. Primus, M. Boutonnet, Phys. Chem. Chem. Phys. 14 (2012) 12970–12981.
[32] N.L. Wu, T.F. Wu, I.A. Rusakova, J. Mater. Res. 16 (2001) 666–669.
[33] Z. Dang, B.G. Anderson, Y. Amenomiya, B.A. Morrow, J. Phys. Chem. 99 (1995) 14437–14443.
[34] L. Li, L. Wang, W. Zhang, X. Zhang, X. Chen, X. Dong, J. Nanopart. Res. 16 (2014) 2753.
[35] K.R. Nemade, R.V. Barde, S.A. Waghuley, Ceram. Int. 41 (2015) 4836–4840.
[36] J.A. Navio, M.C. Hidalgo, G. Colon, S.G. Botta, M.I. Litter, Langmuir 17 (2001) 202–210.
[37] S.G. Botta, J.A. Navio, M.C. Hidalgo, G.M. Restrepo, M.I. Litter, J. Photochem. Photobiol. A 129 (1999) 89–99.
[38] T. Kasnavia, D. Vu, D.A. Sabatini, Ground Water 37 (1999) 376–381.
[39] S. Mubarik, A. Saeed, M.M. Athar, M. Iqbal, J. Ind. Eng. Chem. 33 (2016) 115–121.
[40] Y. Kohno, T. Tanaka, T. Funabiki, S. Yoshida, Chem. Commun. (1997) 841–842.
[41] A.V. Emeline, V.N. Kuznesov, V.K. Ryabchuk, N. Serpone, Environ. Sci. Pollut. Res. 19 (2012) 3666–3675.
[42] T. Rajh, L.X. Chen, K. Lukas, T. Liu, M.C. Thurnauer, D.M. Tiede, J. Phys. Chem. B 106 (2002) 10543–10552.
[43] D.C. Hurum, K.A. Gray, T. Rajh, M.C. Thurnauer, J. Phys. Chem. B 108 (2004) 16483–16487.
[44] S. Liu, N. Zhang, Z.R. Tang, Y.J. Xu, ACS Appl. Mater. Interfaces 4 (2012) 6378–6385.
[45] A.F. Bedilo, M.A. Plotnikov, N.V. Mezentseva, A.M. Volodin, G.M. Zhidomirov, I.M. Rybkina, K.J. Klabunde, Phys. Chem. Chem. Phys. 7 (2005) 3059–3069.